Microstructural Analysis of Bearing Steels by a Statistical Nanoindentation Technique

Esteban Broitman[1], Mohamed Y. Sherif[2], Boris Minov[3], Urszula Sachadel[4]

[1] *Research and Technology Development, SKF B.V., Esteban.Daniel.Broitman@skf.com*
[2] *Research and Technology Development, SKF B.V., Mohamed.Sherif@skf.com*
[3] *Research and Technology Development, SKF B.V., Boris.Minov@skf.com*
[4] *Research and Technology Development, SKF B.V., Urszula.Sachadel@skf.com*

Abstract– The microstructure of ASTM 52100, X30CrMoN15-1, and AISI M62 steel samples, analyzed by optical and scanning electron microscopy and by X-ray diffraction, were correlated to the mechanical properties measured at macro- and nanoscale. The distribution of hardness determined from multiple nanoindentation measurements was deconvoluted, obtaining an estimate of the microstructural constituents, and corresponding plastic and elastic properties at nanoscale.

Keywords – nanoindentation, steel, hardness, statistical nanoindentation, ASTM 52100, X30CrMoN15-1, AISI M62

1. Introduction

The precise knowledge of bearing steel microstructures is of vital importance to understand their tribological performance. Standard microstructural characterization, carried out by optical and electron microscopy together with X-ray diffraction, is usually correlated to the hardness determined by Rockwell or Vickers indentation. The obtained hardness values by these techniques are generally used as a parameter to evaluate the steel resistance against indentation deformation at macro- and microscale. However, the mechanical significance of the steel phases and other microscale inhomogeneities cannot be analyzed by macro and micro-mechanical techniques. The use of instrumented nanoindentation provides a way to measure the mechanical response of these phases at an appropriate scale (~ 10^{-6} m). The use of nanoindentation data together with macro- and microindentation information can be used for multiscale mechanical modelling that could predict the steel mechanical performance for a given composition and microstructure.

Despite of the significant body of research on the hardness of bearing steels at macro- and microscale, their deformation behavior at nanoscale received less attention. Therefore, there is still a need for fundamental understanding of the local deformation behavior of the steels with respect to the local microstructure, which can be used to their optimization. Nanoindentation has been carried out to study individual hard and soft phases in low carbon steel [1], high carbon steel [2], TRIP steels [3], tool steel [4], dual phase steels [5], high speed steel [6], and stainless steel [7].

In the first part of the paper, the background of the indentation techniques to measure hardness of homogeneous materials at macro, micro-, and nanoscale is described. In the second part, the microstructure of ASTM 52100, X30CrMoN15-1, and the powder metallurgy AISI M62 steel samples, analyzed by optical and scanning electron microscopy and X-ray diffraction, are correlated to the mechanical properties measured by multiple nanoindentations. Finally, the distribution of the hardness and modulus of elasticity determined from the nanoindentation observations are deconvoluted, and the results are correlated to the microstructure.

2. Theoretical Remarks

2.1. Indentation Hardness

The hardness of a solid material can be defined as a measure of its resistance to a permanent shape when a constant compressive force is applied. In metals, ceramics, and most of polymers, the hardness is related to the plastic deformation of the surface. Hardness has also a close relation to other mechanical properties like strength, ductility, and fatigue resistance, and therefore, hardness testing can be used in the industry as a simple, fast, and relatively cheap material quality control method [8].

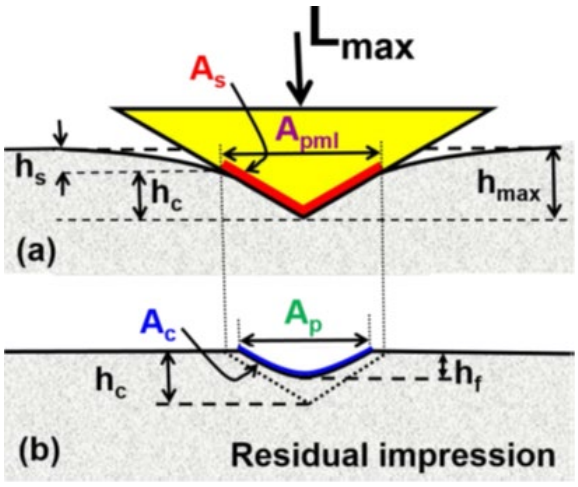

Figure 1: (a) Elasto-plastic deformation at the maximum applied load L_{max}; (b) plastic deformation after releasing the load (Adapted from [8]*).*

At macro- and microscale, the indentation hardness is defined in three different ways, as illustrated in Figure 1. Brinell and Vickers define hardness as the applied load L divided by the actual area A_c of the impressed curved surface. Meyer and Knoop hardness are defined as the ratio of the applied load L to the projected areas A_p of the indent. Finally, the Rockwell, Shore, IHRD, and Buchholz tests determine the hardness by measuring the depth of penetration of an indenter under a large load [8].

At nanoscale, the nanoindentation hardness is defined as:

$$H_{IT} = L_{max} / A_{pml} \qquad (Eq.\ 1)$$

where A_{pml} is the projected area contact at the maximum applied load L_{max} [8]. In this method, the maximum load ranges between few μN and about 500 mN, while penetrations will vary from few nm to about few μm. The indented area results to be very small (nanometer or few micrometers size), and as a consequence, the use of optical microscopy is not possible like in macro- and micro-indentation tests. However, Oliver and Pharr developed in the 1990s a method to accurately calculate hardness H and elastic modulus E from the indentation load-displacement (L-h) data, without need to measure the deformed area [9].

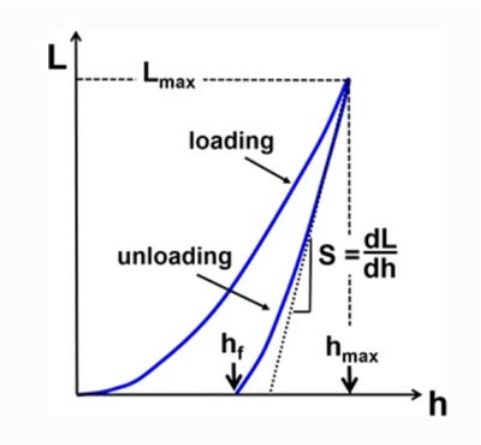

Figure 1: Load–unload curve during nanoindentation (Adapted from [8]).

During the nanoindentation process, the indenter penetrates the sample until a predetermined maximum load L_{max} is reached, with a corresponding penetration depth h_{max}. When the indenter is withdrawn from the sample, the unloading displacement is also continuously monitored until the zero load is reached and a residual penetration depth h_f is measured (Fig. 2). The slope of the upper portion of the unloading curve, S = dL/dh, is called the elastic contact stiffness.

Assuming that pileup is negligible, an elastic model [9] shows that the amount of sink-in h_s (indicated in Fig. 1) is given by:

$$h_s = \varepsilon L_{max}/S \qquad (Eq.\ 2)$$

where ε is a constant that depends on the geometry of the indenter, which for Berkovich and cube-corner indenters has a value ε = 0.75 [9].

The contact depth h_c can be estimated, from figure 1 and eq. 2 as:

$$h_c = h_{max} - h_s = h_{max} - \varepsilon L_{max}/S \qquad (Eq.\ 3)$$

If we assume that we have an ideal Berkovich indenter, the projected area at maximum load A_{pml} can be calculated as:

$$A_{pml} = \sqrt[3]{3}\, tan^2(\alpha/2) h_c^2 = 24.56 h_c^2 \qquad (Eq.\ 4)$$

where α = 130.6° is the angle of the Berkovich indenter [8]. Combining eq. (2), (3), and (4) into equation (1) we obtain:

$$H_{IT} = L_{max} / (h_{max} - \varepsilon L_{max}/S)^2 \qquad (Eq.\ 5)$$

Under the given assumptions, equation (5) shows a way to calculate the hardness of the material using the experimental data from figure 2.

Even if they are carefully manufactured, the indenter tips are usually blunted and/or can have other defects, or they become imperfect after few nanoindentations, so equation (4) is not always valid. In that case, it is necessary to evaluate an empirically determined indenter area function:

$$A_{pml} = f(h_c) = 24.56 h_c^2 + C_1 h^1 + C_2 h^{1/2} + C_3 h_c^{1/3} + \ldots \qquad (Eq.\ 6)$$

where the fitting parameters C_i can be obtained by performing nanoindentation tests on materials with known hardness. The most used material used for the fitting is fused quartz, with a known hardness H = 9.25 GPa [8].

The nanoindentation technique allows also to calculate the elastic modulus of the material by using:

$$S = \frac{2}{B\sqrt{\pi}} E_r \sqrt{A_{pml}} \qquad (Eq.\ 7)$$

where B = 1.034 for indenters of triangular cross-section [8] [9], and E_r is the reduced elastic modulus of the contact defined by:

$$\frac{1}{E_r} = \frac{1-\vartheta^2}{E} + \frac{1-\vartheta_i^2}{E_i} \qquad (Eq.\ 8)$$

where E and ν are the elastic modulus and Poisson's ratio of the sample and E_i and ν_i the elastic modulus and Poisson's ratio of the indenter.

If we try to determine the hardness of homogeneous materials with dimensions of many decimeters (a relatively ''infinite'' material when comparing with the sizes of a macroscale indentation), we probably won't be able to measure different values of indentation hardness measured at different length scales. However, a difference will appear when we try to indent a polycrystalline material with inhomogeneous features of microscale length. While macroscale indentations will give a material average hardness, nanoscale tests can indicate variations in different parts of the sample microstructure because the size of the indentations is usually of few micrometers and the indentation depth can be in the order of tens of nanometers. A nanoindentation can give hardness and elastic modulus variations

in different grains, precipitates, phases and grain boundaries [10].

2.2. Statistical Nanoindentation

2.2.1. Two-phases material

Let's consider a material composed of two phases with different mechanical properties, being phase 2 the "matrix" and phase 1 characterized by a length scale D. (Figure 3).

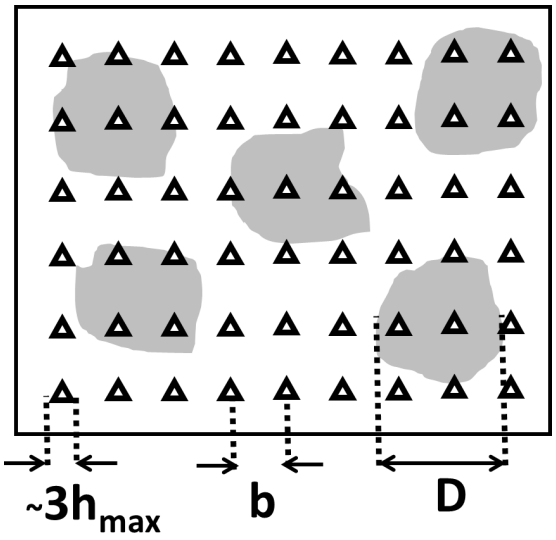

Figure 3: A material with a matrix having one phase with a characteristic size D. The indentations have a size ~3h_{max} and the distance between the indents is b.

If the indentation size (which is ~ 3h_{max} [8]) is much bigger than the than the size D of phase 2 (h_{max} » D), the properties extracted from this indentation will be the average value corresponding to a macro-scale indentation test. On the other hand, if the indentation depth h_{max} is much smaller than the size of phase 2 (h_{max} « D), then a single indentation test in a place far enough from the boundary between the phases can give full information of the phase. In addition, if a large number of tests N (N»1) are done on a grid of distance characteristic b (Figure 3), where b > 10 h_{max} to avoid interference between individual indentation tests, an analysis that includes histograms of mechanical properties can be obtained. Figure 4 is a schematic example of how a histogram (frequency diagram) could be represented for a matrix material of mean hardness H_2 ±σ_2 with a softer phase of mean value H_1 ± σ_1.

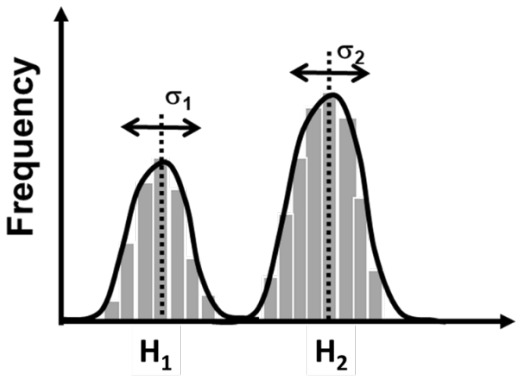

Figure 4: Histogram representing a matrix of hardness H_2 with a softer phase material of hardness H_1..

2.2.2. N-phases material

We can generalize the previous assumption extending to a material of n phases. Let's suppose that each phase i has a mechanical property x (x = H or E) with a discrete histogram of values following a Gaussian distribution. We also assume that the phases do not mechanically interact. The data can be analyzed by deconvoluting the discrete experimental distribution values P(x) of the mechanical property x by the sum of n theoretical probability distribution functions p_i (one for each mechanically different phase:

$$p_i(x) = \frac{1}{\sqrt{2\pi\sigma_i^2}} \exp\left(-\frac{(x-\mu_i)^2}{2\sigma_i^2}\right) \qquad (Eq.\ 9)$$

where μ_i is the arithmetic mean of all Ni values of phase i, while the standard deviation σi or root mean square deviation, is a measure of the dispersion of these values:

$$\mu_i = \frac{1}{N_i} \sum_{k=1}^{N_i} X_k \quad (Eq.\ 10)$$

$$\sigma_i^2 = \frac{1}{N_i - 1} \sum_{k=1}^{N_i} (x_k - \mu_i)^2 \quad (Eq.\ 11)$$

The overall frequency distribution of the mechanical property x will have a probability density function P(x):

$$P(x) = \sum_{i=1}^{n} f_i \; p_i(x) \qquad (Eq.\ 12)$$

where f_i is the volume fraction of the phase i and:

$$\sum_{i=1}^{n} f_i = 1 \quad (Eq.\ 13)$$

From the practical point of view, the function P(x) can be fitted to the experimental data by finding fi, σi and μ_i that are minimizing the standard error:

$$\min \sum_{l=1}^{m} \frac{[y(x_l) - p(x_l)]^2}{m} \qquad (Eq.\ 14)$$

or maximizing R-square, also known as the coefficient of determination (COD), which is calculated as:

$$R^2 = 1 - \frac{\sum_{l=1}^{m}[y(x_l)-p(x_l)]^2}{\sum_{l=1}^{m}\left[y(x_l)-\frac{1}{m}\sum_{l=1}^{m}y(x_l)\right]^2} \quad (Eq.\ 15)$$

where x_l and $y(x_l)$ are the l-th (x,y) coordinates values of the experimental results, and m is the number of "bins" used to build the experimental frequency density. The mean, standard deviation, and volume fraction values of each phase i can be determined by the deconvolution analysis with the condition of minimizing the standard error or R^2.

2.2.3. Selection of indentation depth and number of bins

To identify each of the n-phase property (hardness or elastic modulus), we need to generalize the assumptions of section 2.2.1. In the case of coatings characterization, there is a rule of tomb that the indentation depth should be smaller than the thickness of the coating in order to avoid the influence from the substrate hardness [8]. We can use a similar rule, and establish that, for a multiphase material, the maximum nanoindentation depth needs to be $h_{max} < D/10$, where D is the smallest microstructural length-scale of the material (see figure 3). At the same time, we need also to comply with an inferior limit: $h_{max} > d$, the largest heterogeneity of the indented material.

Different bin sizes can reveal different features of the data. Using a low number of bins will reduce the noise due to sampling randomness but could hide important details about the data distribution; on the other hand, the use of narrow-size bins increases the precision of density estimation but also increases the noise data. There are many methods to estimate the number of bins or their width. We utilize the Freedman-Diaconis rule that determine the number and width by the number of measurements and its spread [11]:

$$Bin\ width = 2\,\frac{IQR(x)}{\sqrt[3]{n}} \quad (Eq.\ 16)$$

where IQR(x) is the interquartile range of the data (i.e., range containing the 50% of all data) and n is the number of measurements.

3. Experimental Conditions

Three quenched and tempered steel samples, ASTM 52100, X30CrMoN15-1, and AISI M62, were selected for the study. The samples were sectioned, ground, polished with 1 µm diamond paste, and then electropolished. Microstructure studies were carried out by optical microscopy using etched specimens (Leica DM6000-M) and by X-ray diffraction (Bruker D8 DISCOVER). The diffractometer was operated at 50 kV and 50 mA, using Zr-filtered Mo Kα1,2 radiation. A step-scan mode was employed over the scanned θ-2θ range of 15-63°, with angular step width of 0.02°, the collection time being for 10 s at each step.

Nanoindentation experiments have been performed with a diamond Berkovich indenter with a tip radius of approximately 150 nm. The employed equipment was a NHT from CSM Instruments (now Anton Paar) with a vertical displacement resolution of 0.01 nm, a force resolution of 0.02 µN, an internal noise uncertainty of 0.3 nm, and thermal drift at room temperature below 0.05 nm/min [12]. Multi-indentations were carried out at L_{max} = 20 mN in grids of 20x25 indents with a space between indents b = 7 µm. It has been shown that the metallographic polishing process can affect nanoindentation results due to the presence of surface roughness and surface mechanical damage [13] [14] [15]. In this work we followed the results of Bublíková *et al*, who demonstrated that a mechanical polishing followed by electropolishing ensures reliable results in nanoindentation experiments and minimizes the indentation size effect for loads higher than 5 mN [15].

4. Results and Discussion

4.1. Optical Microscopy

Figure 5 shows the steel microstructures. Figure 5a exhibits a typical ASTM 52100 bearing steel microstructure with an uneven distribution of carbides, while the X30CrMoN15-1 steel (Figure 5b) reveals that they are well distributed. The AISI M62 steel microstructure (Figure 5c) displays the presence of several carbides clusters.

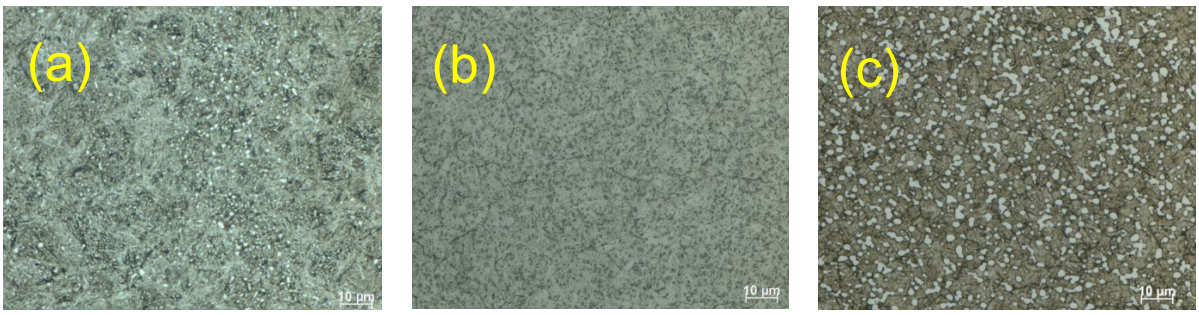

Figure 5 Microstructure of (a) ASTM 52100, (b) X30CrMoN15-1, (c) AISI M62.

Table 1: A summary of the Rietveld refinement results in wt.%. (*) Amount is too small to be certain of the phase's presence.

	ASTM 52100	X30CrMoN15-1	AISI M62
α-Fe (matrix)	86.2 ± 0.1	76.8 ± 0.6	75.9 ± 0.4
Austenite	6.4 ± 0.1	1.8 ± 0.1	2.2 ± 0.5
Cementite	7.4 ± 0.1	-	-
Fe_2Mo_4C (M_6C)	-	-	9.4 ± 0.1
VC	-	-	4.3 ± 0.1
Fe_3W_3C (M_6C)	-	-	7.7 ± 0.3
Mo2C hexagonal	-	0.1 ± 0.1(*)	0.4 ± 0.4
Cr_7C_3	-	20.2 ± 0.4	-

4.2. XRD analysis

Two X-ray spectra were acquired per microstructure, and the Rietveld method was used to identify and quantify phases present (Table 1). For the ASTM 52100 steel, the calculated retained austenite content was 6.4±0.1 wt.%. However, for the AISI M62 and X30CrMoN15_ microstructures, very small amount of retained austenite was found at 1.8±0.1 and 2.2±0.5 wt.%, respectively. The AISI M62 microstructure was estimated to contain also a total of 17.1 wt.% of the M6C-type of carbide on average, as well as 4.3±0.1 wt.% vanadium carbide.

4.3. Indentation Hardness and Elastic Modulus

The macroscale hardness of the steels, measured by Vickers (10 kgf) and by Rockwell C (150 kgf) according to standards ISO 6507-1 [13] and ISO 6508-1 [14], respectively, are shown in Table 2. The moduli of elasticity E displayed in the table have been provided by the steel suppliers. The nanoindentation hardness H_{IT} and elastic modulus E_{IT} in Table 2 are calculated as the mean value and corresponding error of 500 measurements. For the elastic modulus calculation, a Poisson's ratio value of 0.30 has been assumed for the three steels.

Even if Vickers and nanoindentation hardness are measured in the same scale (MPa), it should be noted that the values cannot be directly compared. Vickers hardness HV is calculated as the maximum applied load L_{max} divided by the contact area A_c of the indent after the indenter has been released, while the nanoindentation hardness H_{IT} is calculated as L_{max} divided by the projected contact area A_{pml} of the indent *at the maximum load* (see Figure 1). A geometrical equivalence between A_c and A_{pml} can be established only in materials that fully deform plastically, which is not the case for steels.

Table 2: Macro- and nanoscale mean values of hardness and elastic modulus for the three steel microstructures.(*) Elastic modulus values E at macroscale provided by the steel suppliers.

	HV10 (MPa)	HRC (150 kgf)	E* (GPa)	H_{IT} (MPa)	E_{IT} (GPa)
ASTM 52100	7280 ± 30	61.4 ± 0.1	210	8184 ± 59	212.7 ± 1.1
X30CrMoN15-1	6850 ± 20	58.4 ± 0.2	223	7970 ± 150	221.4 ± 2.3
AISI M62	9230 ± 80	67.9 ± 0.1	241	9690 ± 190	260.9 ± 4.3

Figure 6 is an example of the load-displacement curves for the average hardness nanoindentation of the three studied steels: (a) ASTM 52100, (b) X30CrMoN15-1, (c) AISI M62. The Hertzian elastic contact deformation solution curve, deduced from Hertz theory equation [15]:

$$L = \frac{4}{3} E_r R^{1/2} h^{3/2} \qquad (Eq.17)$$

(where R is the radius of the indenter) is also indicated as a dotted line. Since neither a rapid slope change in the loading curves nor pop-out elbows in the unloading curves were observed in all indentations, it is deduced that no deformation-induced transformations have been triggered during the nanoindentation.

4.4. Statistical Indentation Results

Figures 7 (a-c) display the nanoindentation hardness histograms for ASTM 52100, X30CrMoN15-1 and AISI M62 steels, respectively. The hardness histogram for ASTM 52100 (Figure 7a) reveals four different deconvoluted peaks, at 6.76, 8.14, 9.17, and 9.63 GPa. The X30CrMoN15-1 steel shows a pronounced peak centered at 8.94 GPa, plus a wide peak at about 5.06 GPa (Fig. 7b). Finally, the AISI M62 steel peaks were found at 10.03 and 6.09 GPa (Fig. 7c). The number of peaks in all histograms, which are found by fitting multiple Gaussian peaks and maximizing the coefficient of determination R-square as explained in section #2.2, are not only correlated with the phases identified by X-ray analysis (Table 1) but also related to the complexity of the observed microstructures (Figure 5).

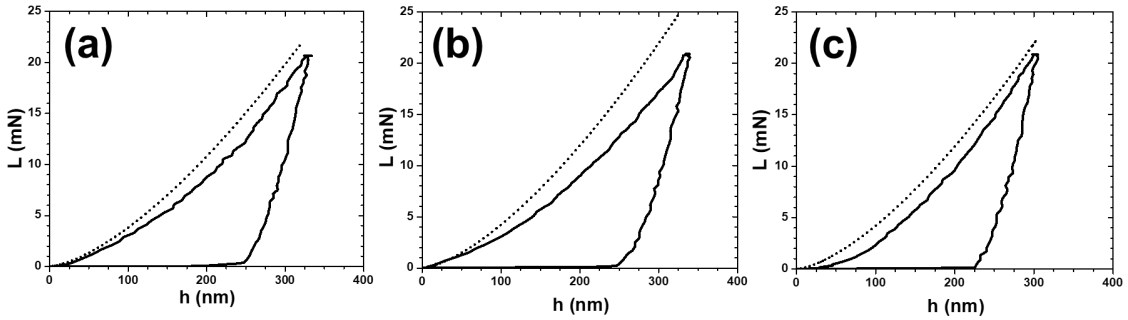

Figure 6: Nanoindentation load-displacement curve for (a) ASTM 52100, (b) X30CrMoN15-1, (c) AISI M62 (full line) and the corresponding theoretical elastic Hertz solution curve (dotted line).

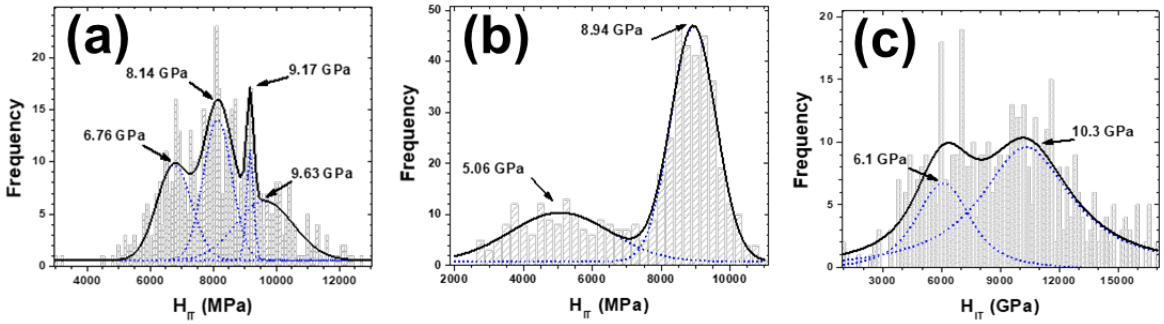

Figure 7: Microstructure of (a) ASTM 52100, (b) X30CrMoN15-1, (c) AISI M62.

There has been some steel studies showing multi-indent nanoindentation hardness histograms for DP980 [5] [16], multiphase Q&P [17], AISI 304L stainless [18], and dual-phase [19] steels. However, all these studies concentrated only on showing individual phases distributions without any analysis. A more elaborated use of statistical nanoindentation to study multiphase phase distribution has only be done for stainless steel [20] [21] and SM490 steel [22]. Haušild *et al* studied the distribution of the phases at different stainless steel deformation levels; they observed that the Gaussian hardness peaks moved to higher values with the increase of deformation, in agreement with results obtained by using x-ray diffraction during *in-situ* tensile testing [20]. Roa *et al* studied the dependence of nanoindentation hardness with crystallographic orientation of austenite grains in metastable stainless steels [21]. They correlated the data of each indentation with electron backscatter diffraction (EBSD) characterization to conclude that the hardness of (001) and (101) grains were lower than (111) grains. Finally, Pham and Kim studied the welded zones of SM490 steel [22]. They found out that the weld zone contained three phases: low stiffness ferrite, high stiffness ferrite, and pearlite. While all the aforementioned authors studied different steels, all agree in the idea that the hardness for the different phases observed by the statistical nanoindentation analysis were consistent with results from other methods found in the literature.

When we compare the results of statistical analysis in Figure 7 with the results found by X-ray diffraction (XRD) analysis (Table 1) we can notice that the number of phases apparently does not coincide. For instance, for ASTM 52100 we found 5 peaks (Figure 7a), but the Rietveld refinement results show the presence of only 3 phases. We need to consider that, in fact, the histograms reflect not only the response from the phases in the sample, but also the effect of grain boundaries, different grain sizes and orientations, non-uniform chemical distributions and dislocation density within grains. Furthermore, our approach in Section #2.2 considers phases that follow a simple mixing rule; in fact, the mixing rule should be more complicated as it will depend on non-linear stress distribution around the indentation zone.

However, the results shown in Figure 7 can be interpreted as a characteristic fingerprint for each steel. From this point of view, the nanoindentation statistical analysis can be considered as a kind of “hardness spectroscopic analysis” where each steel will show an own number of characteristic “peaks” centered in characteristic “hardness” values. Following this spectroscopy analogy, Haušild results [20] showing that the center of the steel Gaussian hardness peak moves according to the deformation of the sample, and Roa results [21] describing how the position of the Gaussian hardness peak depends on the orientation of the phase, behave in a similar fashion to what is observed for the same phenomena through the corresponding XRD peak shifts.

5. Conclusions

A statistical nanoindentation technique has been used for first time to compare three different bearing steel microstructures. The distribution of the mechanical properties determined from multiple nanoindentation measurements was deconvoluted. The results show that this nanoindentation technique can be used to generate hardness histograms that reflect unique characteristics (fingerprints) for the different bearing steel mechanical properties.

6. Bibliography

[1] I. de Diego-Calderón, M. J. Santofimia, J. M. Molina-Aldareguia, M. A. Monclús und I. Sabirov, "Deformation behavior of a high strength multiphase steel at macro- and micro-scales," *Materials Science and Engineering: A,* Bd. 611, pp. 201-211, 2014.

[2] R. Hossain, F. Pahlevani, M. Z. Quadir und V. Sahajwalla, "Stability of retained austenite in high carbon steel under compressive stress: an investigation from macro to nano scale," *Scientific Reports,* Bd. 6, p. 34958, 2016.

[3] Q. Furnémont, M. Kempf, P. J. Jacques, M. Göken und F. Delannay, "On the measurement of the nanohardness of the constitutive phases of TRIP-assisted multiphase steels," *Materials Science and Engineering: A,* Bd. 328, Nr. 1-2, pp. 26-32, 2002.

[4] F. Pöhl, A. Weddeling und W. Theisen, "Mechanical Characterization of Hard Phases by Means of Nanoindentation," in *Proceedings of the International Symposium on Wear Resistant Alloys for the Mining and Processing Industry CBMM*, Campinas, 2018.

[5] M. D. Taylor, K. S. Choi, X. Sun, D. K. Matlock, C. E. Packard, L. Xu und F. Barlat, "Correlations between nanoindentation hardness and macroscopic mechanical properties in DP980 steels," *Materials Science and Engineering: A,* Bd. 597, pp. 431-439, 2014.

[6] H. Zhu, Q. Zhu, A. Kosasih und A. K. Tieu, "Investigation on mechanical properties of high speed steel roll material by nanoindentation," *Materials Research Innovations,* Bd. 17, pp. 35-39, 2013.

[7] S. Chen, Y. Miyahara und A. Nomoto, "Crystallographic orientation dependence of nanoindentation hardness in austenitic phase of stainless steel," *Philosophical Magazine Letters,* Bd. 98, Nr. 11, pp. 473-485, 2018.

[8] E. Broitman, "Indentation Hardness Measurements at Macro-, Micro-, and Nanoscale: A Critical Overview," *Tribology Letters,* Bd. 65, p. 23, 2017.

[9] W. Oliver und G. Pharr, "An improved technique for determining hardness and elastic modulus using load and displacement sensing indentation experiments," *Journal of Materials Research,* Bd. 7, Nr. 6, p. 1564–1583 , 1992.

[10] A. C. Fischer-Cripps, Nanoindentation, New York: Springer-Verlag , 2011.

[11] D. Freedman und P. Diaconis, "On the histogram as a density estimator: L2 theory," *Probability Theory and Related Fields,* Bd. 57, Nr. 4, p. 453–476, 1981.

[12] Anton Paar, Mechanical Characterization of Materials, Ostfildern: Anton Paar, 2016.

[13] S. Pathak, D. Stojakovic, R. Doherty und S. R. Kalidindi, "Importance of surface preparation on the nano-indentation stress-strain curves measured in metals," *Journal of Materials Research,* Bd. 24, Nr. 3, pp. 1142-1155, 2009.

[14] M. C. Wurz, F. Pape, M. Wark und H. H. Gatzen, "Investigation of Liquid Additives on the Nano-Hardness of NiFe during Polishing," *Tribology Online,* Bd. 6, Nr. 1, pp. 113-116, 2011.

[15] P. Bublíková, H. K. Namburi und D. Marušáková, "Optimization of Surface Properties for Nanoindentation Studies on Nuclear Structural Materials," *Materials Science Forum,* Bd. 891, pp. 67-72 , 2017.

[16] International Organization for Standardization, "ISO 6507-1-2005: Metallic Materials—Vickers Hardness Test—Part 1: Test Method," International Organization for Standardization, Geneva, 2005.

[17] International Organization for Standardization, "ISO 6508-1: Metallic Materials - Rockwell Hardness Test - Part 1: Test Method," International Organization for Standardization, Geneva, 2016.

[18] H. Hertz, "Über die Berührung fester elastischer Körper (On the contact of elastic solids)," *Journal für die reine und angewandte Mathematik,* Bd. 92, pp. 156-171, 1881.

[19] G. Cheng, F. Zhang, A. Ruimi, D. P. Field und X. Sun, "Quantifying the effects of tempering on individual phase properties of DP980 steel with nanoindentation," *Materials Science and Engineering A,* Bd. 776, pp. 240-49, 2016.

[20] G. Cheng, K. S. Choi, X. Hu und X. Sun, "Determining individual phase properties in a multi-phase Q&P steel using multi-scale indentation tests," *Materials Science and Engineering A,* Bd. 652, pp. 384-395, 2016.

[21] K. S. Mao, C. Sun, Y. Huang, C.-H. Shiau, F. A. Garner, P. D. Freyer und J. P. Wharry, "Grain orientation dependence of nanoindentation and deformation-induced martensitic phase transformation in neutron irradiated AISI 304L stainless steel," *Materialia,* Bd. 5, p. 100208, 2019.

[22] A. Khosravani, C. M. Caliendo und S. R. Kalidindi, "New Insights into the Microstructural Changes During the Processing of Dual-Phase Steels from Multiresolution Spherical Indentation Stress–Strain Protocols," *Metals,* Bd. 10, p. 18, 2020.

[23] P. Haušild, V. Davydov, J. Drahokoupil, M. Landa und P. Pilvin, "Characterization of strain-induced martensitic transformation in a metastable austenitic stainless steel," *Materials & Design,* Bd. 31, Nr. 4, pp. 1821-1827, 2010.

[24] J. J. Roa, G. Fargas, A. Mateo und E. Jiménez-Piqué, "Dependence of nanoindentation hardness with crystallographic orientation of austenite grains in metastable stainless steels," *Materials Science and Engineering A,* Bd. 645, pp. 188-195, 2015.

[25] T.-H. K. S.-E. Pham, "Determination of mechanical properties in SM490 steel weld zone using nanoindentation and FE analysis," *Journal of Constructional Steel Research,* Bd. 114, pp. 314-324, 2015.

[26] International Organization for Standardization, "ISO 6508-1: Metallic Materials—Rockwell Hardness Test—Part1: Test Method," International Organization for Standardization, Geneva, 2016.